Design and Modeling of a Nanomechanical Sensor Using Silicon Photonic Crystals

Chengkuo Lee, *Member, IEEE*, Rohit Radhakrishnan, Chii-Chang Chen, Jing Li, Jayaraj Thillaigovindan, and N. Balasubramanian

***Abstract*—Conventionally a line defect in the photonic crystal (PhC) is used to create a waveguide for light propagation through the PhC. A PhC based filter is designed by introducing micro-cavities within the line defect so as to form the resonant bandgap structure for PhC. Such a PhC waveguide (PhCWG) filter shows sharp resonant peak in output wavelength spectrum. We proposed a suspended silicon bridge structure comprising this PhCWG filter structure. Since the output resonant wavelength is sensitive to the shape of air holes and defect length of the micro-cavity. Shift of the output resonant wavelength is observed for suspended PhCWG beam structure under particular force loading. In other words, the induced strain modifies the shape of air holes and the spacing among them. Such an effect leads to shift of resonant wavelength. Under optical detection limitation of 0.1 nm for resonant wavelength shift, the sensing capability of this nanomechanical sensor is derived as that vertical deformation is 20–25 nm at the center and the smallest strain is 0.005% for defect length. This innovative design conceptualizes a new application area for PhCs, i.e., the nanometer-scale physical sensors for strains and forces.**

***Index Terms*—Microelectromechanical systems (MEMS), nanoelectromechanical systems (NEMS), nanomechanical sensor, nanophotonics, photonic crystals (PhCs).**

I. Introduction

In recent years, nanometer scale photonic crystals (PhCs) are attractive optical structures for controlling and manipulating the flow of light. Various devices such as smaller optical waveguides, microscopic optical cavities and the photonic bandgap structures, open up various possibilities for novel photonic devices. Silicon-photonics-based active devices including photodetectors, modulators, and lasers have been demonstrated [1], [2]. On the other hand, optical technologies play a cornerstone role in chemical and biochemical analysis nowadays. For example, optical chemical sensing based on guided-wave devices has been trapped considerable attention. Different integrated optical chemical and biochemical sensors have been proposed, such as those using directional couplers [3], Mach–Zehnder interferometers [4], Bragg gratings [5], and microring resonators [6]. The sensing mechanism is mainly attributed to detection of effective refractive index change in terms of homogeneous sensing, i.e., influenced by cover medium refractive index modification, or surface sensing, i.e., interfered by thickness change of thin biomolecular layer immobilized on surface [7].

Obviously, PhC is an even more attractive sensing platform, because two-dimensional (2-D) silicon-based PhCs typically comprise a group of air holes and the local electromagnetic field is modified by surface state of air holes. Thus, PhC-based chemical and biochemical sensors are extremely sensitive to a small refractive index change produced by bio-molecules immobilization on the hole walls. The change of surface state of inner wall of holes introduces much more strong influence on the propagating light than the small interaction between evanescent field and the analyte at the waveguide surface. Recently, Lee and Fauchet have demonstrated the detection of 2.5 fg of protein coated on inner sidewalls of holes of a two-dimensional silicon PhC device by measuring the resonant wavelength shift of output spectrum [8]. The measurement of ambient induced refractive index change of glycerol–water mixture in various ratios was first demonstrated by Chow *et al.* in 2004 [9]. Based on detecting the resonant wavelength shift, PhCs have been applied to detecting gold nanoparticles of 10 nm in diameter [10] and sensing ion concentration absorbed in ion-selective polymer covered on PhCs [11].

In addition to the scientific exploration of applying PhCs as ultrasensitive biochemical and chemical sensors, Suh *et al.* has proposed a new displacement sensing mechanism based on due to photon tunneling and Fano interference in two slabs of PhC. The transmission contrast of 20 dB is obtained regarding to a distance change between the two PhC slabs for about 1% of operating wavelength [12], [13]. Levy *et al.* have proposed a novel displacement sensor comprising two planar photonic crystal waveguides (PhCWGs) aligned along the same axis of light propagation. The output light intensity is strongly dependent on the alignment accuracy, i.e., the coupling efficiency between input and output PhCWGs. Any deformation of structure, i.e., considering as displacement, will lead to misalignment so as to reduce the output light intensity. They provided simulation results to prove this device concept [14]. Based on a similar concept of two PhCWGs where one in stationary and the other is movable, Xu *et al.* placed an air hole on both sides of PhCWGs

Manuscript received June 7, 2007; revised November 13, 2007. This work was partially supported by grants from a joint-funded research project based on Faculty Research Fund R-263-000-358-112/133 and R-263-000-475-112 of the National University of Singapore and from the Institute of Microelectronics, Agency for Science, Technology and Research (A*Star), Singapore.

C. Lee is with the Department of Electrical and Computer Engineering, National University of Singapore, Singapore 117576, Republic of Singapore, and also with the Institute of Microelectronics, Agency for Science, Technology and Research (A*STAR), Singapore 117685, Republic of Singapore (e-mail: elelc@nus.edu.sg; leeck@ime.a-star.edu.sg).

R. Radhakrishnan and J. Thillaigovindan are with the Department of Electrical and Computer Engineering, National University of Singapore, Singapore 117576, Republic of Singapore.

C.-C. Chen is with the Department of Optics and Photonics, National Central University, Jhong-Li, 320, Taiwan, R.O.C.

J. Li and N. Balasubramanian are with the Institute of Microelectronics, Agency for Science, Technology and Research (A*STAR), Singapore 117685, Republic of Singapore.

Color versions of one or more of the figures in this paper are available online at http://ieeexplore.ieee.org.

Digital Object Identifier 10.1109/JLT.2007.915273

and created an optical resonator structure with Q-factor of 40. The resulted intensity reduction in output port is in linear proportion to the longitudinal displacement between PhCWGs [15]. Moreover, Pursiainen *et al.* created a flexible three-dimensional (3-D) PhC by using a self-assembly fabrication process. This flexible 3-D PhC contains multishelled polymer spheres of high-refractive-index and absorbing materials filled in the interstitial space surrounding said spheres. The dimension of this device is a 1-cm-wide strip film. This device was placed on top of a sample holder and was uniformly stretched in micrometer scale while the optical property is measured *in situ*. They demonstrated a result of 50% reduction of transmission intensity at only 1% strain that is corresponding to about a 5-nm wavelength shift of the resonant peak in the reflection spectrum [16]. However, good discrimination of resonant wavelength shift regarding to 1% strain may not be easily due to a very low quality factor of the resonant wavelength peak. Recently EI-Kady *et al.* proposed a new device concept of detecting submicron crack of substrates based on using a 3-D PhC structure as the physical sensor. It was reported that a PhC sensor was attached on a polymer substrate. According to the simulated results derived by using the finite-difference time-domain (FDTD) approach, this PhC sensor experienced changes in its bandgap profile when micro-damage is induced in the said substrate [17].

Interestingly, either the intensity reduction of output peak or resonant wavelength shift has been deployed as the sensing scheme for PhC-based physical sensors, i.e., displacement and strain sensors. Thus, we measure the change in optical signals and correlate such changes with physical parameters, like displacements and strains. For instance, 1% strain represents about 1–5-nm deformation in the hole diameter for silicon 2-D PhC devices. Since the typical size of point defects, i.e., air holes, in silicon PhC is about 100–450 nm, it implies silicon-PhC-based physical sensors should exhibit outstanding performance intrinsically. However, while the recent progress of PhC-based biochemical and chemical sensors has opened a new R&D arena, the physical sensors using PhC structures demand much more effort to drive the experimental results to the stage of proof-of-concept. It is worthwhile to mention that movable suspended silicon waveguides of 1 μm have been applied to modify the resonator characteristics of a microtoroidal structure [18]. It is an example of deploying microelectromechanical systems (MEMS) technology for enabling tunble nano/microphotonics. However, in this paper, we proposed a free-standing bridge beam structure comprising PhCWG for strain and force sensing, where a beam structure is a common mechanical structure used in MEMS based physical sensors. Thus, we apply the resonator characteristics of PhCWG for sensing strain and loaded force. This new concept of nanomechanical sensor will open a new window for a new research field of optical nanoelectromechanical systems (NEMS).

II. Configuration and Modeling of PhCWG Microresonator Devices

The term of PhC means a subclass of materials where a periodic modulation of the refractive index (RI) exists for a given material. PhCs may possess a photonic bandgap (PBG) upon the exact periodic modulation. Thus, a given bandwidth of light

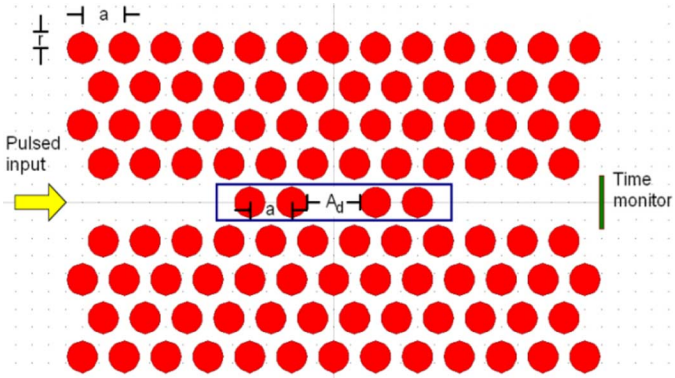

Fig. 1. Layout drawing of PhCWG using hexagonal array of holes, with lattice constant "a", A_d is the distance between two holes in the center of micro-cavity (defect length), and "r" is the radius of the cavity. Pulsed light is launched from the left (arrow) and the output is measured at the right (time monitor).

cannot be transmitted through such material. A PhCWG is considered as a planar PhC with a line defect in the periodic structure, where a line defect is considered as a silicon waveguide typically [19]. The basic property of a PhCWG is that a given bandwidth of light can be guided in the silicon waveguide as the light is confined laterally by the PhC and vertically by total internal reflection (TIR), in which it is similar to conventional waveguide structures. On the other hand, four air holes, i.e., a sort of point defects, have been introduced at the center of said silicon waveguide of PhCWG to form a resonator structure. It is reported that two of high-Q resonances centered at wavelengths 3.621 and 3.843 μm. The quality factors of these two resonant wavelength peaks were measured as 640 and 190, respectively [20]. Sandoghdar *et al.* have applied scanning near-field optical microscopy (SNOM) to visualize the optical intensity topography around these four air holes of this microresonator structure. The peak intensity of resonance shown at 3.84 μm has been observed [21]. These evidences point out that silicon PhCWG with four air holes along the embedded silicon waveguide is a good design of optical resonator. In our proposed device configuration, we deploy this four-hole-based microresonator structure as our fundamental design. As shown in Fig. 1, the PhCWG is formed by a regular array of air holes in a silicon substrate with a hexagonal lattice structure of period and the lattice constant of a $=$ 500 nm. The radius of all holes in the structure is r $=$ 180 nm. A linear waveguide is created by removing a column of air holes among the hexagonally arranged holes patterns. We insert one pair of two air holes into the linear waveguide as two reflectors, i.e., four holes in total. Thus, a point defect is defined between the two reflectors to form a micro-cavity. The width of the micro-cavities is defined as the defect length, i.e., A_d, the spacing between the pair of two holes as shown in Fig. 1. The length and width of this PhCWG are $l = 6.4$ μm and $w = 4.8$ μm. By performing the planewave expansion method, we can obtain the normalized frequency of the photonic bandgap for the TE mode exists between 0.28 and 0.32. The corresponding bandgap in wavelength is between 1563 and 1786 nm. The 2-D FDTD method is performed to simulate the propagation of the electromagnetic waves in the waveguides. The lithography and etching based CMOS fabrication technology have been reported to be good at making PhC

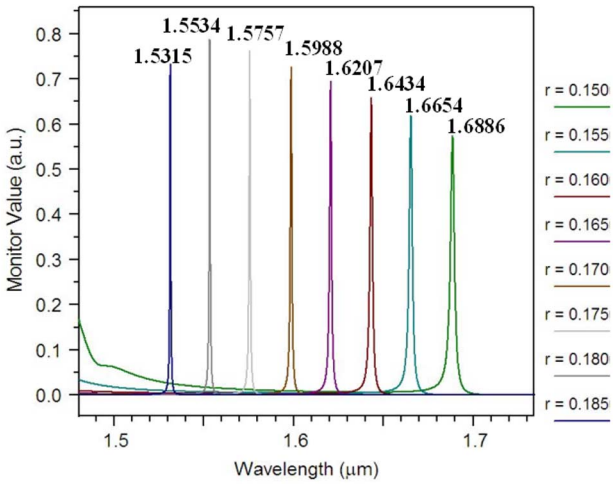

Fig. 2. Calculated shift in the resonant wavelength versus various hole radii from 150 to 185nm.

structure from a SOI (silicon-on-insulator) wafer [22]. A silicon SOI substrate with device layer of 200 nm and a SiO_2 insulation layer of 1 μm is selected as the basic device configuration first. We conduct the simulation throughout the whole study upon this assumption. In contrast to the case of the layout dimensions used in [20] and [21], i.e., designing for resonant wavelengths in far infrared region, we optimize our PhCWG designs to enable the output resonant wavelength peaks appeared in the wavelength range of 1550 to 1620 nm, i.e., the near-infrared region. The common optical spectrum analyzer (OSA) used in optical communication industry can give us down to a 0.1-nm resolution of measuring resonant wavelength within this region.

As we highlighted in previous paragraphs, the resonant wavelength of PhCWG is strongly affected by surface state of holes. For the SOI wafer with the air holes, there are three regions in consideration for the calculation of the effective refractive index, viz. air above the wafer (n_1), silicon device layer (n_2), and underlying silicon oxide layer (n_3). The respective refractive indexes are $n_1 = 1.0$, $n_2 = 3.46$, and $n_3 = 1.48$. Kawano and Kitoh have described a way of calculating effective refractive index [23]. Solving for the principal electromagnetic fields in the y direction and applying appropriate boundary conditions at interface of silicon and SiO_2, the effective refractive index (n-eff) was found to be 2.74 for silicon device layer thickness of $t = 200$ nm. When we deploy effective refractive index (n-eff) of 2.74 and lattice constant (a) of 500 nm for simulation, the output resonant wavelength peaks versus hole radii from 150 to 185 nm are shown in Fig. 2. It is observed that shift in resonant wavelength towards shorter wavelength with respect to increment in the radius of air holes.

III. Optimization of Device Configuration of Nanomechanical Sensor Using PhCWG Microresonator

In order to apply the PhCWG to creating a MEMS structure that is sensitive to deformation or deflection under an applied force, we proposed a suspended bridge beam with PhCWG along the center as shown in Fig. 3(a) and (b). Regarding to the fabrication process, the PhCWG structure is defined by deep

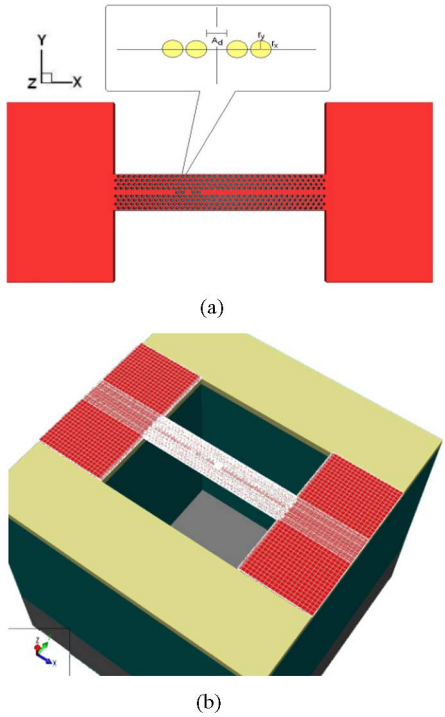

Fig. 3. (a) Top view of the bridge structure with length, $l = 20$ μm, width, $w = 5$ μm, thickness of the silicon bridge, $t = 200$ nm. The inset shows structure of the reflectors. (b) Top view of the entire device.

UV photolithography and front side silicon DRIE (deep reactive ion etching) technique first. Thereafter, we may also apply the silicon DRIE and wet chemical etching to remove the underneath silicon and SiO_2 insulation layer from the backside, respective. Thus, we will have a suspended bridge beam comprising PhCWG structure as illustrated in Fig. 3(b) eventually. As we mentioned that the effective refractive index is highly sensitive to the thickness of device layer and the surface state as well, we need to calculate effective refractive index (n-eff) for suspended silicon beam in which it is considered as "air–Si–air" configuration instead of "air–Si–SiO_2"configuration in conventional silicon waveguide case, i.e., discussed in previous section. The derived effective refractive index is 2.6916. The effective refractive index is highly sensitive to the thickness of device layer. It has been observed that such a decrement in the effective refractive index leads to shift in the resonant wavelength toward shorter wavelength region. For example, in the design of a $= 500$ nm and $r = 180$ nm, the resonant wavelength is shifted from 1553.3 to 1529.4 nm for the PhCWG beam structure changing from configuration of "air–Si–SiO_2" to configuration of "air–Si–air," respectively.

In addition to the lattice constant "a", the hole radius "r", effective refractive index, number of air holes to form the two reflectors, and the defect length A_d are also critical to the resonant wavelength and Q factor of resonant peak. Moreover, we need to consider the influence contributed by the displacement and deformation of the these holes along x and y directions and elongation of the PhCWG in x and y directions, when the said suspended PhCWG beam structure is under deformation due to externally applied force. In other words, for the operation of this nanomechanical sensor as either a strain sensor or a force sensor,

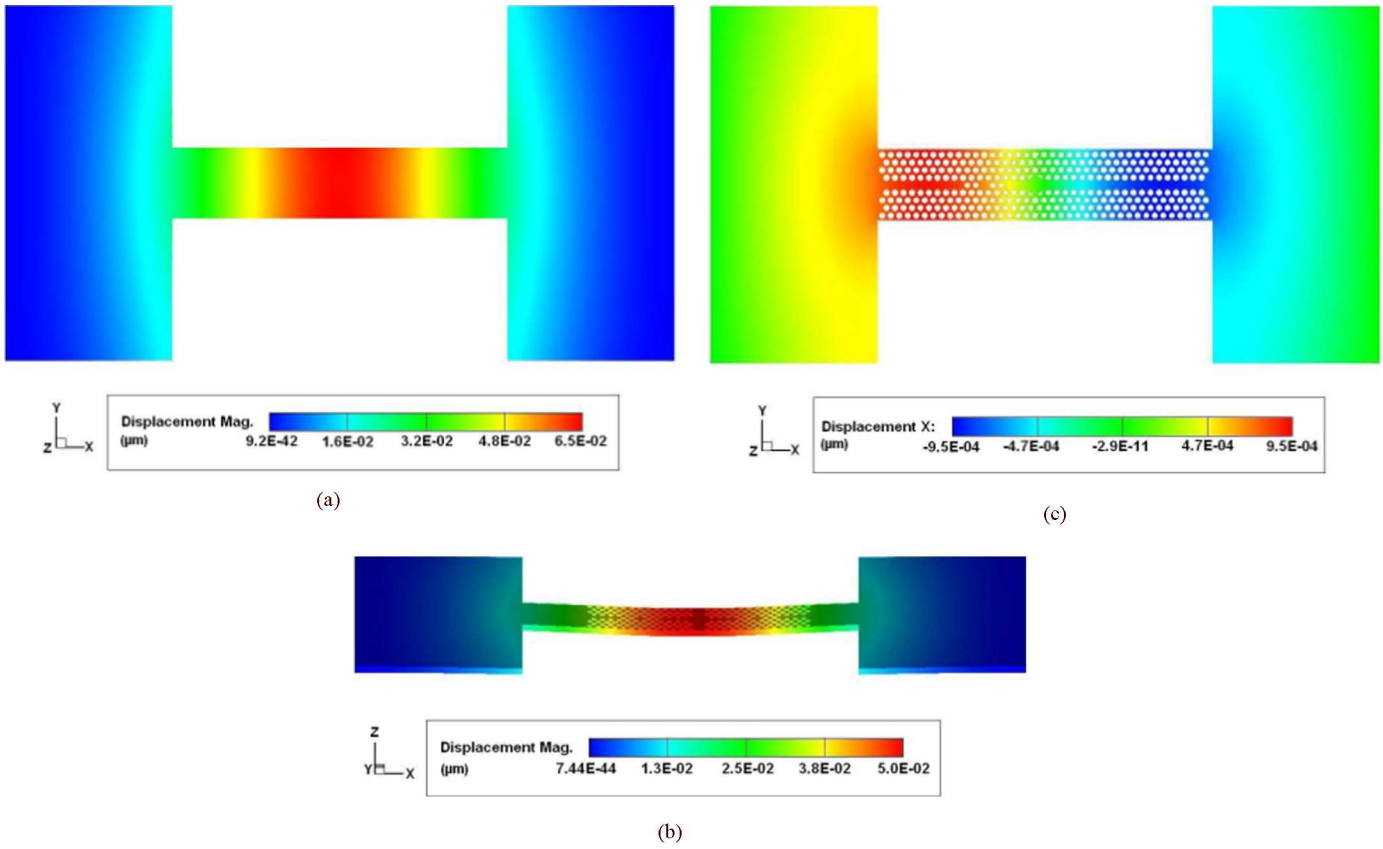

Fig. 4. (a) Loaded bridge showing displacement (magnitude) in the z direction (into the plane of paper) for an applied normal force (z direction), $F = 0.79\ \mu$N. As shown by the color bar, maximum displacement in the z direction is at the center (red), and the two blue regions show the fixed ends of the bridge structure with minimal displacement. (b) Bridge structure of PhCWG showing the deflection in the z direction for the same applied force. The deflection has been shown with an exaggeration of 10 in the visual. The horizontal is shown by the thick black line at the bottom, clearly showing the curved shape of the released beam upon application of force. All displacements are measured in μm. (c) Bridge structure of PhCWG showing the displacement of each point on the bridge along x direction upon application of force, $F = 0.79\ \mu$N at the center of the bridge into the plane of the paper. The displacement in the x direction increases as the distance from the center and the beam ends increases. Max change in A_d is seen at a distance of 3 μm from the center (small yellow bar closer to the center of the beam).

it is important that changes of certain physical parameters have to be taken into account upon applied force. We have conducted the simulation and concluded that a point defect comprising two reflectors in which each reflector contains two air holes is the optimized configuration. Thus, we stay with this four-hole-based configuration as a parameter in optimization work of nanomechanical sensor without considering the "number of air holes to form the two reflectors." Besides, the schematic drawing of reflectors comprising four holes with radii in the x and y directions and defect length is shown in the inset of Fig. 3(a).

Assuming there is no change in r_x and r_y, it was noted that the 0.2-nm increase in the defect length caused a 0.14-nm increase in the resonant wavelength, whilst it was seen that a 1-nm increase in elongation or displacement of these four holes in the y direction individually, i.e., no change in A_d and r_x, resulted in a minute resonant wavelength shift toward short wavelength region. In contrast to cases of elongation or displacement that happened along the y direction, a 1-nm elongation of these four holes along the x direction $(r'_x = r_x + 0.5)$ leads a resonant wavelength shift of 0.93 nm toward the short-wavelength region. It was concluded from this study that a change in the defect length coupled with an elongation and/or deformation in the x direction would be the most sensitive parameters to resonant wavelength shift. As a result, to make the PhCWG device sensitive to change of strain or applied force, it would be necessary to design and layout the PhCWG along a direction such that the device would experience the force along the x direction as much as possible.

According to aforementioned considerations, a PhCWG bridge structure as shown in Fig. 3(b) was optimized in terms of deformation sensitivity for being a strain sensor or a force sensor. Dimensions of this suspended bridge are as follows: length of 20 μm, width of 5 μm, and thickness of 200 nm. Initially, we need to check the strain distribution along this suspended beam structure. We built up a 3-D solid model by using commercial finite-element method (FEM) software, i.e., CoventorWare.[1] While current study is aiming at exploring feasibility and optimizing the design, in the next step, we will fabricate this novel nanomechanical photonic strain sensor based on designs derived in this paper. The front-side bulk silicon micromaching is considered as the approach to undercut the bulk silicon and release the PhCWG bridge structure. To successfully release the beam of 5 μm, an undercut of 3 μm at both ends of substrate is typically required. Thus, we include a 3-μm undercut at both sides of silicon substrate at end of bridge. It means the actual deformable length is taken as 26 μm along the longitudinal direction in the FEM model. In the future, we

[1][Online] Available: http://www.coventor.com/coventorware/

plan to deploy an atomic force microscopy (AFM) cantilever tip to introduce a particular amount of force on the center of a suspended beam so as to create vertical deformation and strain in reflectors area. In view of such an approach, the contacting spot of the AFM cantilever tip on the center beam is assumed as 500 nm in diameter. Therefore, we may define the force load in terms of pressure. For instance, a constant pressure of 1 to 5 MPa is calculated as 0.7 to 4 μN with regard to a loading area of 500-nm diameter, i.e., 7.85×10^{-13} m^2.

Thus, in the FEM simulation, we apply a pressure load of 1.0 MPa, e.g., calculated as 0.785 μN, at the center of suspended beam in the z direction (into the plane of the beam). A displacement of this beam along z direction is shown in Fig. 4(a). The topographic colors represent various degrees of vertical deformation. Fig. 4(b) exhibits the oblique view of a bridge structure embedded with PhCWG under the same pressure load. The center of the beam is displaced the most in the z direction as shown by the red color in Fig. 4(a) and (b). Fig. 4(c) shows the deformation of each point on the bridge in the x direction. It is seen here that the deformation increases with distance increasing from the center of the beam and reduces again as it approaches the fixed ends of the beam. It is observed that the change in defect length reaches maximum at a distance of 3 μm from the center of the beam. This is shown by the yellow and orange regions in Fig. 4(c). We derived this particular position by placing these four-hole reflectors at different position along the longitudinal direction of beam and checking the largest change in A_d and r_x. In other words, the drastic change of vertical position means largest strain area or largest deformation along the longitudinal direction of beam. We arranged the two reflectors of four holes at this 3-μm point in order to take advantage of that this position will lead our PhCWG exhibits the most sensitive behavior regarding to strain and force. Since the induced strain will be perfectly reflected in the change of A_d and r_x so as to gain in largest resonant wavelength shift. As shown in Fig. 4(c), the optimized position of the PhC was selected at the region at which the change in defect length was a maximum.

Again, in the FEM simulation, we introduced deformation of beam structure under pressure of to 1–5 MPa with a 1-MPa difference between each two tries. Upon the topographic data as shown in Fig. 4(c), we may derive relative changes in r_x and r_y for all the holes and A_d, r_x and r_y for micro-cavity. Then such derived parameters are fed into commercial software for conducting FDTD simulation, i.e., RSoft. Finally, we derived the resonant wavelength shift based on the simulated output spectrum. Besides, we noticed that very sensitive behavior of resonant wavelength shift versus loading force is observed in the small loading force region. As a result, we conducted comprehensive simulation work in this region. The simulation has been conducted in more detailed analysis for cases of loading pressure from 1 to 2 MPa with a 0.2-MPa difference between two data points.

IV. Characteristics of Nanomechanical Sensor

Fig. 5 shows the simulated various resonant wavelength peaks with respect to different applied pressure from 1 to 2 MPa with a 0.2-MPa increment of each step. The shift to

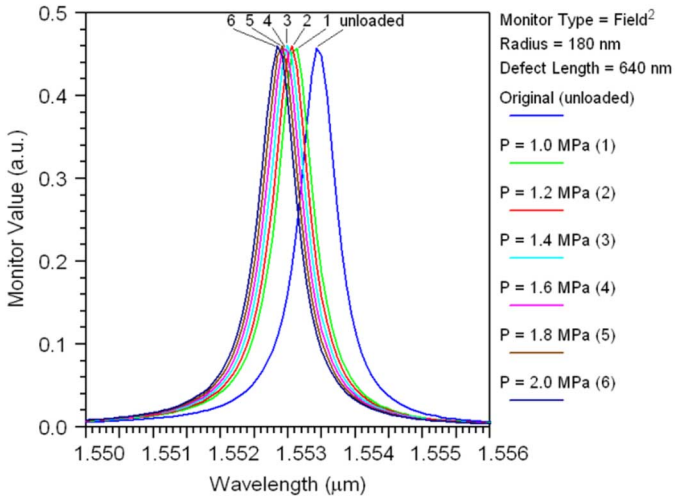

Fig. 5. Shift in the resonant peak due to force applied (1.0 MPa–2.0 MPa in steps of 0.20 MPa).

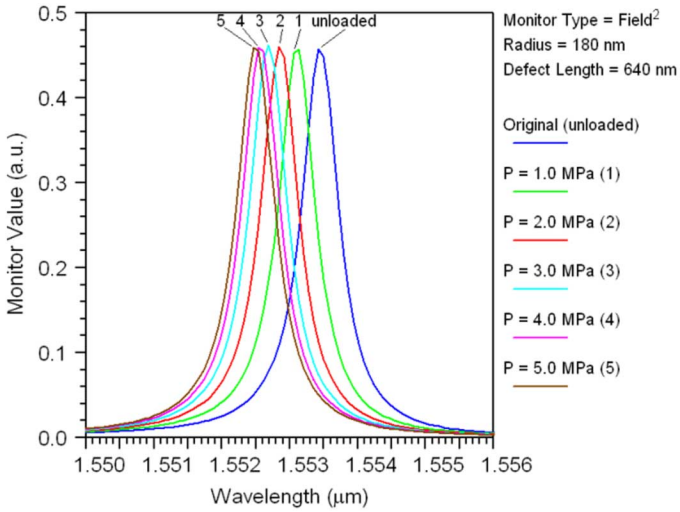

Fig. 6. Shift in the resonant peak due to force applied (1.0–5.0 MPa in steps of 1.0 MPa).

shorter wavelengths corresponds directly to the reduction in A_d and an elongation of r_x. Besides, the actual shifts in the resonant wavelength after simulations by said FDTD method for loading pressure from 1 to 5 MPa with a 1-MPa increment of each step can be determined from Fig. 6, i.e., the derived resonant wavelength peaks. We may combine the data points shown in Figs. 5 and 6 and present such data in terms of loading force as shown in Fig. 7. The initial defect length A_d and radius r are 640 and 180 nm, respectively. Within the range of 0.7- to 1.7-μN loading force, rather linear behavior observed for the shift of resonant wavelength regarding to the applied force. For force loads between 2 μN and 4 μN, it is seen that the relationship is best described by a second-order equation. For the overall data, a polynomial regression line of degree two fits well with the data points. The resonant wavelength shift is derived as a function of vertical deflection at center of suspended beam, as shown in Fig. 8. It shows that a second-order equation can fit this data points, while the minimum detectable vertical deflection is measured as about 20–25 nm in terms of 0.1-nm

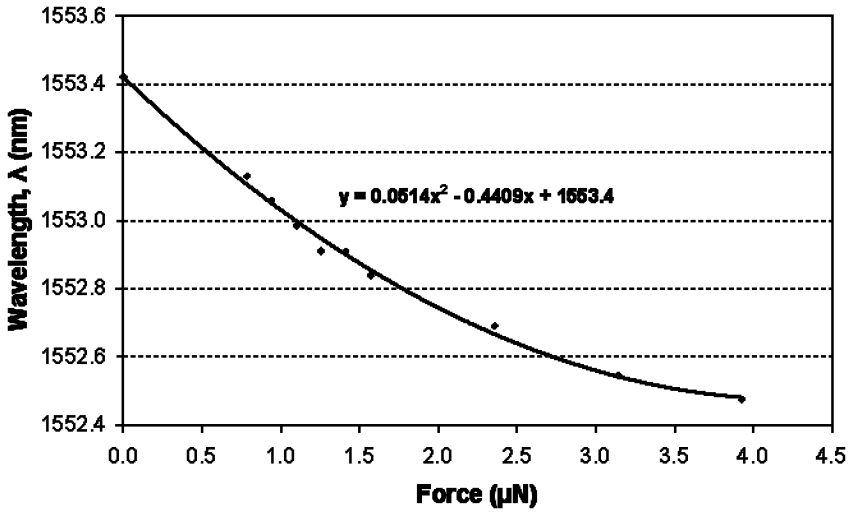

Fig. 7. Force applied on suspended beam versus resonant wavelength shift of PhCWG.

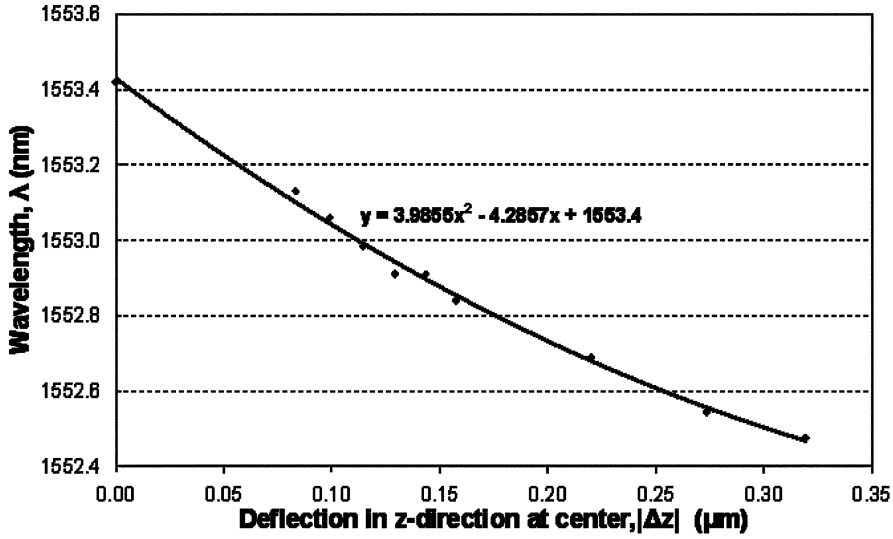

Fig. 8. Deflection in the z direction versus resonant wavelength shift of PhCWG.

resonant wavelength shift. A relatively linear relationship is observed for vertical deflections from 75 to 160 nm. In consideration of that the deformation which is the most sensitive resonant wavelength shift is defect length, i.e., A_d, the strain in PhCWG is defined as a ratio of the change in defect length, i.e., ΔA_d, to the original A_d. In other words, it is the percentage change in the defect length. Fig. 9 shows the relationship between the shift in resonant wavelength of the PhCWG and the absolute value of strain. Although another polynomial regression line of degree two fits the overall data perfectly, it is also observed that the change in resonant wavelength fits in linear behavior for strain within 0.03%, referring to red dashed line. Again the detectable smallest strain is derived as 0.005%. It is a significant improvement with three orders of magnitude than previous strain sensing data reported by [16].

We also need to explore the temperature effect because the refractive index of silicon has known to be sensitive to ambient temperature. To characterize the resonant wavelength shift corresponding to the temperature drift, we need to consider two major effects. First of all, the change in defect length due to volume expansion attributed to increased temperature should be evaluated. By using the FEM approach, we derived the volume change of radius and defect length first. The resulted shift in resonant wavelength is simulated as ± 0.05 nm for 25 °C $\pm$ 10 °C. Second, the refractive index of silicon at temperatures deviated from room temperature, i.e., considered as 25 °C, can be calculated by using the approach reported by McCaulley *et al.* [24]. Thereafter, the resulted shift in resonant wavelength is simulated as ± 0.43 nm for 25 ° C $\pm$ 5 °C and ± 0.12 nm for 25 °C $\pm$ 1 °C. It means we only need to consider the second effect, i.e., silicon refractive index deviation versus temperature drift. It also implies that a temperature stabilizer, e.g., thermoelectric-cooler, is required to maintain the PhCWG nanomechanical sensors at an ambient temperature with drift within ± 1 °C. Thus, the PhCWG nanomechanical sensors can detect the resonant wavelength shift in the 0.1-nm resolution.

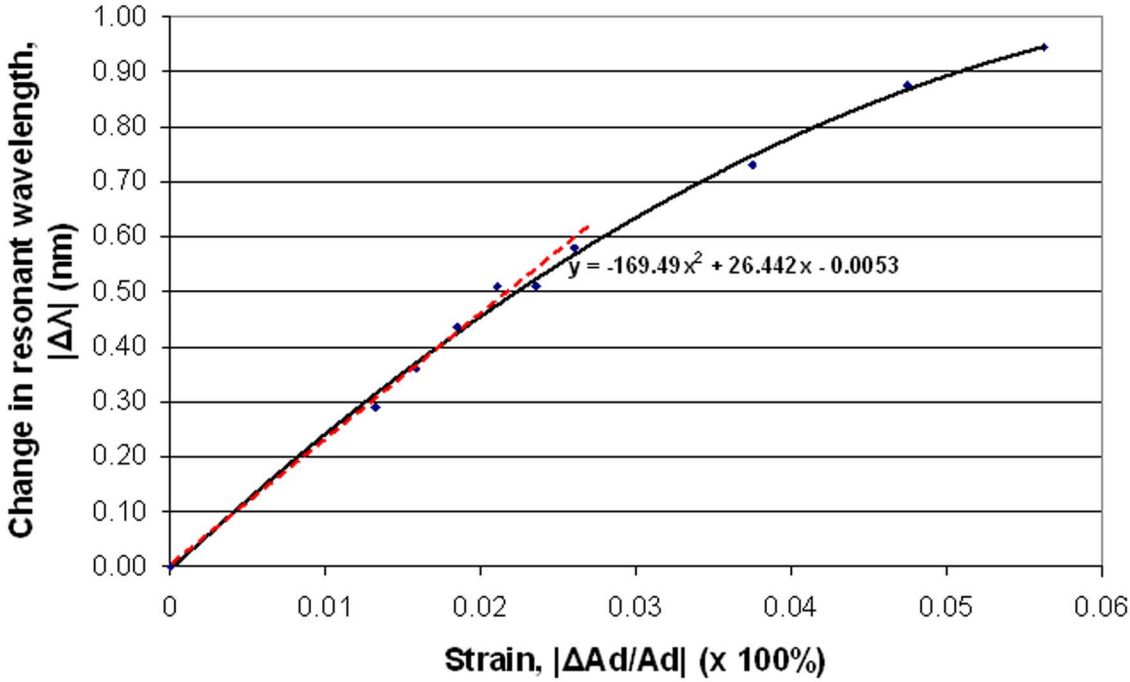

Fig. 9. Induced strain of A_d versus resonant wavelength shift of PhCWG.

V. Concluding Remarks

The force and strain sensing capability of a novel PhCWG based bridge structure has been studied. We insert one pair of two air holes into the silicon linear waveguide as two reflectors. A point defect, i.e., a micro-cavity, is defined between the two reflectors. By introducing such a point defect, this suspended beam structure becomes a PhCWG based nanophotonic filiter. It generates a clear resonant wavelength peak with a Q factor as high as 1000. The deformation of the suspended beam could be detected by measuring the resonant wavelength shift. Longitudinal deformation of air holes and a change in defect length of the micro-cavity contribute resonant wavelength shift effectively. In terms of the percentage change in the defect length due to loading force, such strain can be detected as low as 0.005% with regard to a force load of 0.25 μN. It concludes that the minimum detectable force and the minimum detectable vertical deflection are 0.25 μN and 20–25 nm, respectively.

To benchmark the sensitivity of the proposed PhCWG nanomechanical sensor, we may refer the data of conventional sensors in the force and displacement detection category. The first example is a bulk micromachined silicon piezoresistive pressure sensor with a diaphragm of epitaxial layer. With a diaphragm size of about 1 mm^2, the maximum detectable force is 25 mN versus pressure of 15 PSI. The accuracy is 0.5% within the full scale in which it results with a force detection accuracy of 100 μN [25]. The second example that should be addressed is the atomic force microscope (AFM) using a micromachined cantilever sensor. For a normal AFM based on the optical level detection scheme [26], the minimum detectable displacement is in the Angstroms level, while the minimum detectable force is in the range of nN to pN depending on the stiffness of cantilever. In addition, the AFM using the piezoelectric PZT cantilever sensor can also achieve a displacement resolution of 1.5 Å [27]. Therefore, the further improvement of the detection limit of the present device design is desirable, when we consider the possibility of commercialization.

In summary, the derived simulation results show that this device concept could be applied to the force sensing, strain detection, and displacement measurement. The main advantage provided by this new sensing concept is an ultracompact device footprint. Simply speaking, the applications may be ultra-compact gyroscopes, accelerometers, and biosensors, etc. This new nanomechanical sensor will explore a new research field of optical NEMS.

References

[1] H. Benisty, J.-M. Lourtioz, X. Checoury, S. Combrie, and A. Chelnokov, "Recent advances toward optical devices in semiconductor-based photonic crystals," *Proc. IEEE*, vol. 94, pp. 997–1023, 2006.

[2] B. Jalali and S. Fathpour, "Silicon photonics," *J. Lightw. Tech.*, vol. 24, no. 12, pp. 4600–4600, Dec. 2006.

[3] B. J. Luff, R. D. Harris, J. S. Wilkinson, R. Wilson, and D. J. Schiffrin, "Integrated-optical directional coupler biosensor," *Opt. Lett.*, vol. 21, pp. 618–618, 1996.

[4] F. Prieto, B. Sepulveda, A. Calle, A. Llobera, C. Domynguez, A. Abad, A. Montoya, and L. M. Lechuga, "An integrated optical interferometric nanodevice based on silicon technology for biosensor applications," *Nanotechnol.*, vol. 14, pp. 907–907, 2003.

[5] W. C. L. Hopman, P. Pottier, D. Yudistira, J. v. Lith, P. V. Lambeck, R. M. D. L. Rue, and A. Driessen, "Quasi-one-dimensional photonic crystal as a compact building-block for refractometric optical sensors," *IEEE J. Sel. Top. Quantum Electron.*, vol. 11, no. 1, pp. 11–11, Jan.–Feb. 2005.

[6] C. Y. Chao, W. Fung, and L. J. Guo, "Polymer microring resonators for biochemical sensing applications," *IEEE J. Sel. Top. Quantum Electron.*, vol. 12, no. 1, pp. 134–134, Jan.–Feb. 2006.

[7] F. Dell'Olio and V. M. N. Passaro, "Optical sensing by optimized silicon slot waveguides," *Opt. Express*, vol. 15, pp. 4977–4977, 2007.

[8] M. Lee and P. M. Fauchet, "Two-dimensional silicon photonic crystal based biosensing platform for protein detection," *Opt. Express*, vol. 15, pp. 4530–4530, 2007.

[9] E. Chow, A. Grot, L. W. Mirkarimi, M. Sigalas, and G. Girolami, "Ultracompact biochemical sensor built with two-dimensional photonic crystal microcavity," *Opt. Lett.*, vol. 29, pp. 1093–1093, 2004.

[10] B. Schmidt, V. Almeida, C. Manolatou, S. Preble, and M. Lipson, "Nanocavity in a silicon waveguide for ultrasensitive nanoparticle detection," *Appl. Phys. Lett.*, vol. 85, pp. 4854–4856, 2004.
[11] S. Chakravarty, J. Topol'ancik, P. Bhattacharya, S. Chakrabarti, Y. Kang, and M. E. Meyerhoff, "Ion detection with photonic crystal microcavities," *Opt. Lett.*, vol. 30, pp. 2578–2578, 2005.
[12] W. Suh, M. F. Yanik, O. Solgaard, and S. Fan, "Displacement-sensitive photonic crystal structures based on guided resonance in photonic crystal slabs," *Appl. Phys. Lett.*, vol. 82, pp. 1999–2001,, 2003.
[13] W. Suh, O. Solgaard, and S. Fan, "Displacement sensing using evanescent tunneling between guided resonances in photonic crystal slabs," *J. Appl. Phys.*, vol. 98, pp. 033102,–033102,, 2005.
[14] O. Levy, B. Z. Steinberg, N. Nathan, and A. Boag, "Ultrasensitive displacement sensing using photonic crystal waveguides," *Appl. Phys. Lett.*, vol. 86, pp. 104102–104102, 2005.
[15] Z. Xu, L. Cao, C. Gu, Q. He, and G. Jin, "Micro displacement sensor based on line-defect resonant cavity in photonic crystal," *Opt. Express*, vol. 14, no. 1, pp. 298–305, 2006.
[16] O. L. J. Pursiainen, J. J. Baumberg, K. Ryan, J. Bauer, H. Winkler, B. Viel, and T. Ruhl, "Compact strain-sensitive flexible photonic crystals for sensors," *Appl. Phys. Lett.*, vol. 87, pp. 101902–101902, 2005.
[17] I. EI-Kady, M. M. R. Taha, and M. F. Su, "Application of photonic crystals in submicron damage detection and quantification," *Appl. Phys. Lett.*, vol. 88, pp. 253109–253109, 2006.
[18] J. Yao, D. Leuenberger, M.-C. M. Lee, and M. C. Wu, "Silicon microtoroidal resonators with integrated MEMS tunable coupler," *J. Lightw. Technol.*, vol. 13, no. 2, pp. 202–208, Mar.–Apr. 2007.
[19] S. G. Johnson, P. R. Villeneuve, S. Fan, and J. D. Joannopoulos, "Linear waveguides in photonic-crystal slabs," *Phys. Rev.*, vol. B 62, pp. 8218–8222, 2000.
[20] P. Kramper, A. Birner, M. Agio, C. M. Soukoulis, F. Müller, U. Gösele, J. Mlynek, and V. Sandoghdar, "Direct spectroscopy of a deep two-dimensional photonic crystal microresonator," *Phys. Rev.*, vol. B 64, pp. 233102–1, 2001.
[21] P. Kramper, M. Kafesaki, C. M. Soukoulis, A. Birner, F. Müller, R. Wehrspohn, U. Gösele, J. Mlynek, and V. Sandoghdar, "Near-field visualization of light confinement in a photonic crystal microresonator," *Opt. Lett.*, vol. 29, pp. 174–176, 2004.
[22] W. Bogaerts, R. Baets, P. Dumon, V. Wiaux, S. Beckx, D. Taillaert, B. Luyssaert, J. Van Campenhout, P. Bienstman, and D. Van Thourhout, "Nanophotonic waveguides in silicon-on-insulator fabricated with CMOS technology," *J. Lightw. Technol.*, vol. 23, no. 1, pp. 401–412, Jan. 2005.
[23] K. Kawano and T. Kitoh, *Introduction to Optical Waveguide Analysis: Solving Maxwell's Equations and The Schrödinger Equation*. New York: Wiley, 2001.
[24] J. A. McCaulley, V. M. Donnelly, M. Vernon, and I. Taha, "Temperature dependence of the near-infrared refractive index of silicon, gallium arsenide, and indium phosphide," *Phys. Rev. B*, vol. 49, no. 11, pp. 7408–7417, 1994.
[25] T. Kenny, "Nanometer-scale force sensing with MEMS devices," *IEEE Sensors J.*, vol. 1, no. 2, pp. 148–157, Aug. 2001.
[26] F. J. Giessibl, "AFM's path to atomic resolution," *Mat. Today*, vol. 8, no. 5, pp. 32–41, 2005.
[27] C. Lee, T. Itoh, R. Maeda, and T. Suga, "Characterization of micromachined piezoelectric PZT force sensors for dynamic scanning force microscopy," *Rev. Sci. Instrum.*, vol. 68, no. 5, pp. 2091–2100, 1997.

Chengkuo Lee (S'93–M'96) received the M.S. degree in materials science and engineering from National Tsing Hua University, Hsinchu, Taiwan, R.O.C., in 1991, the M.S. degree in industrial and system engineering from Rutgers University, New Brunswick, NJ, in 1993, and the Ph.D. degree in precision engineering from the University of Tokyo, Tokyo, Japan, in 1996.

He worked as foreign researcher in the Nanometer-scale Manufacturing Science Laboratory at the Research Center for Advanced Science and Technology (RCAST) of the University of Tokyo from 1993 to 1996. He had also worked in the Mechanical Engineering Laboratory, AIST, MITI of Japan as a JST Research Fellow in 1996. Thereafter, he was a Senior Research Staff Member of Microsystems Laboratory, Industrial Technology Research Institute (ITRI), Hsinchu, Taiwan, R.O.C. In September 1997, he joined the Metrodyne Microsystem Corporation, Hsinchu, Taiwan, R.O.C., and established the MEMS device division and the first micromachining fab for commercial purposes in Taiwan. He was the Manager of the MEMS device division between 1997 and 2000. He was an Adjunct Assistant Professor in the Electro-physics Department of National Chiao Tung University, China, in 1998, and an Adjunct Assistant Professor in the Institute of Precision Engineering of the National Chung Hsing University, China, from 2001 to 2005. He co-founded Asia Pacific Microsystems, Inc. (APM) Hsinchu, Taiwan, R.O.C., in August 2001, and he became the Vice President of R&D, then later until the end of 2005, the VP of optical communication business unit and Special Assistant of CEO in charge of international business and technical marketing for MEMS foundry service at APM, Inc., one of the top 30 MEMS manufacturers in the world in recent years. Currently, he is an Assistant Professor at the Department of Electrical and Computer Engineering of the National University of Singapore and a Senior Member of Technical Staff at the Institute of Microelectronics (IME), Agency for Science, Technology and Research (A∗STAR), Singapore. He has contributed more than 80 international conference papers and extended abstracts, 45 peer-reviewed international journal articles, and 8 U.S. patents in MEMS and Nanotechnology field.

Dr. Lee is the member of the Materials Research Society (MRS), and the Institution of Electrical Engineers (IEE) Japan.

Rohit Radhakrishnan received the B.Sc. degree from the Department of Electrical and Computer Engineering at the National University of Singapore in 2007.

He is currently an Executive in the Commercial Department of BW Shipping Managers Pte Ltd., Singapore.

Chii-Chang Chen, photograph and biography not available at the time of this publication.

Jing Li received the Bachelor's of Engineering and Master's of Engineering degrees in electrical and electronic engineering from Xi'an Jiaotong University (XJTU), China, in 1995 and 1998, respectively, and the Ph.D. degree from the School of Electrical and Electronic Engineering, Nanyang Technological University (NTU), Singapore, in 2006.

Currently, she is a Senior Research Engineer with the Institute of Microelectronics (IME), Singapore. Her research interests include optical MEMS, inertia MEMS, optical communications, optical module package, and microsystems.

Jayaraj Thillaigovindan received the Bachelor's degree in electrical and electronics engineering from PSG College of Technology, India, in 2004. He is currently working towards the M.Sc. degree from the Department of Electrical and Computer Engineering at the National University of Singapore in May 2008.

N. Balasubramanian, photograph and biography not available at the time of publication.